Radiation-induced double strand breaks and subsequent apoptotic DNA fragmentation in human peripheral blood mononuclear cells

MYRIAM GHARDI[1], MARJAN MOREELS[1], BERNARD CHATELAIN[2], CHRISTIAN CHATELAIN[2] and SARAH BAATOUT[1]

[1]Radiobiology Unit, Molecular and Cellular Biology, Belgian Nuclear Research Centre,
SCK•CEN, B-2400 Mol; [2]Laboratory of Experimental Hematology and Oncology,
UCL Mont-Godinne University Hospital, B-5530 Yvoir, Belgium

Abstract. In case of accidental radiation exposure or a nuclear incident, physical dosimetry is not always complete. Therefore, it is important to develop tools that allow dose estimates and determination that are based on biological markers of radiation exposure. Exposure to ionizing radiation triggers a large-scale activation of specific DNA signaling and repair mechanisms. This includes the phosphorylation of γH2AX in the vicinity of a double-strand break (DSB). A DNA DSB is a cytotoxic form of DNA damage, and if not correctly repaired can initiate genomic instability, chromosome aberrations, mutations or apoptosis. Measurements of DNA DSBs and their subsequent repair after *in vitro* irradiation has been suggested to be of potential use to monitor cellular responses. The bone marrow and the blood are known to be the most radiosensitive tissues of the human body and can therefore be of particular importance to find radiation-induced biological markers. In the present study, changes in H2AX phosphorylation and apoptosis of irradiated human peripheral blood mononuclear cells (PBMCs) were analyzed. Freshly isolated PBMCs from healthy donors were irradiated with X-rays (0.1, 0.25, 0.5, 1, 2 and 4 Gy). The phosphorylation of γH2AX was measured at different time points (0, 0.25, 1, 2, 4, 6 and 24 h) after irradiation. We detected a linear dose-dependency of γH2AX phosphorylation measured by γH2AX foci scoring using immunofluorescence microscopy as well as by γH2AX fluorescence detection using flow cytometry. Apoptosis was detected by measuring DNA fragmentation at different time points (0, 24, 48, 72, 96 h) after X-irradiation using DNA ladder gel electrophoresis. The apoptotic DNA fragmentation increased in a dose-dependent manner. In conclusion, DNA DSBs and subsequent apoptotic DNA fragmentation monitoring have potential as biomarkers for assessing human exposure in radiation biodosimetry.

Introduction

The most critical lesion induced by ionizing radiation is the interruption of genome integrity by DNA double-strand breaks (DSBs), which represents potentially lethal damage to the cell (1-4). In response to DSB generation, histone H2AX, a subfamily of histone H2A, is rapidly phosphorylated on Ser-139 (γH2AX) by members of the phosphoinositide 3-kinase (PI3-K) family [ataxia telangiectasia mutated Rad3-related (ATR), ataxia telangiectasia mutated (ATM)], and DNA-dependent protein kinase (DNA-PK) (5). The phosphorylation of thousands of molecules of H2AX in the chromatin adjacent to the DSB site is one of the earliest known events in response to radiation-induced DSB (6). After DSB formation, cells activate DNA damage checkpoint pathways to stop cell division in order to repair the damage and promote survival of the cell. Proteins important in cell cycle arrest, such as p53 and checkpoint kinases 1 and 2, are activated by ATR and ATM kinases immediately after DSB induction (2,7).

Antibodies to γ-H2AX allow the visualization of a 'focus' at the DSB site. Due to the ease of this visualization, measuring γH2AX has become a standard method for detecting the induction and repair of DNA DSB. Traditionally, these foci have been quantified using immunofluorescence microscopy. However, with increasing sample numbers, high throughput assays can be advantageous. Flow cytometry methods have been developed and are ideal for measuring γH2AX in a high number of cells. Besides detection of γH2AX foci by microscopy, the relative expression of γH2AX as measured by flow cytometry has been shown to be a useful and reliable indicator of DNA damage as well (8,9).

Radiation-induced DSBs are repaired within a few hours following irradiation. Many proteins are involved in various stages of DSB repair (10-13) thereby accumulating in the

Correspondence to: Dr Marjan Moreels, Radiobiology Unit Molecular and Cellular Biology, Belgian Nuclear Research Centre, SCK•CEN, B-2400 Mol, Belgium
E-mail: mmoreels@sckcen.be

region of γH2AX. Their mutual interaction at the site of DSBs is crucial for correct repair (14).

The global response of a cell to DNA damage triggers multiple pathways involved in sensing DNA damage, activating cell cycle checkpoints and inducing DNA repair (15). However, when the damage is severe, cellular apoptosis can be induced.

Since both strands are damaged, DSBs are more difficult to repair compared to single base damage or single-strand DNA breaks. Generally, DSBs are assumed to be the most important lesion to induce apoptosis (16). For this reason all living organisms possess the ability to detect even a few, possibly a single DSB (17,18) and communicate this information to the cell cycle. However, specific slowly repaired or unrepaired DSB may eventually be responsible for induction of apoptosis.

Human peripheral blood mononuclear cells (PBMCs), which constitute a sample of non-proliferating normal tissue cells in the G0 phase within the body, are obtained by minimally invasive means and the large numbers of cells can be serially obtained in a short time.

The purpose of this study is to evaluate γH2AX foci and radiation-induced apoptosis as biodosimeter candidates and to determine a possible consistency of data regarding radiation-induced DNA damage and the radio-induced apoptosis in terms of cytotoxicity. In the present study, we used the γH2AX staining to detect DNA-DSB in human lymphocytes irradiated in fluorescence microscopy and in flow cytometry. These experiments were performed at low, moderate and high doses (0.1, 0.25, 0.5, 1, 2 and 4 Gy) of X-rays and the kinetics of γH2AX foci within 24 h after irradiation were studied to monitor the subsequent repair of radiation-induced DNA damage. Furthermore, radiation-induced apoptosis was assessed by the measurement of apoptotic fragmentation in irradiated PBMCs from 24 h until 96 h after irradiation.

Materials and methods

Sample collection. Blood samples were collected by venipuncture in EDTA-vacutainer tubes (Becton-Dickinson, Belgium) from healthy donors (non-smokers, 20-40 years of age) from whom informed consent was obtained prior to the experiments.

Isolation of peripheral blood mononuclear cells (PBMCs). PBMCs were isolated from volunteers' blood by gradient density centrifugation using Histopaque-1077 (Sigma-Aldrich, Belgium) according to the manufacturer's instructions. After washing in cold phosphate-buffered saline (PBS, Gibco, Belgium), the cells were resuspended at a density of $2x10^6/ml$ in culture flasks in RPMI-1640 medium (Gibco) supplemented with 10% fetal bovine serum (FBS, Gibco) and 1% penicillin-streptomycin (Invitrogen, Belgium). The cell suspension was maintained in an incubator at 37°C humidified with 5% CO_2 until irradiation.

In vitro irradiation, culture and harvesting. The cells were irradiated at room temperature with 0.1, 0.25, 0.5, 1, 2 and 4 Gy of X-rays. The irradiation was performed with a Pantak HF420 RX machine operating at 250 kV, 15 mA, 1 mm Cu filtration and at a dose rate of 0.26 Gy/min (SCK•CEN, Belgium). Non irradiated control samples were included

under similar experimental conditions. After irradiation, cells were incubated (37°C, 5% CO_2) and further processed after different time points (from 15 min until 96 h). Biological endpoints included DSB repair (γH2AX), internucleosomal DNA fragmentation (DNA ladder) and determination of the apoptotic index (TUNEL).

Measurement of γH2AX foci by immunofluorescence microscopy. At different time points (0.25, 4 and 24 h) after X-irradiation, PBMCs, were cytospun on coverslips, air-dried and fixed in 4% formaldehyde (Invitrogen,) in PBS. Unirradiated control samples were included as well. Coverslips were washed 3 times for 5 min in PBS, permeabilized for 5 min at room temperature with 0.2% Triton X-100 in PBS containing 3% bovine serum albumin (BSA, Gibco), and then blocked in 3% BSA-PBS for 30 min at room temperature. Cells were thereafter incubated for 1 h at 37°C with a primary antibody (mouse anti-H2A.X, phospho (Ser139) monoclonal antibody, Abcam, UK) for γH2AX diluted (1:300) in 3% BSA-PBS. The cells were washed 3 times with PBS and incubated with a secondary fluorescein isothiocyanate (FITC)-conjugated goat anti-mouse (Sigma-Aldrich) diluted 1:250 in 3% BSA-PBS for 1 h at room temperature in the dark. After 3 washings in cold PBS, cells were mounted in a mounting medium (Vectashield® Mounting Medium, Vectashield, Vector Laboratories, UK) containing DAPI (4,6-diamidino-2-fenilindole), a counterstain for DNA.

The immunofluorescence images were captured with an automated Nikon TE2000E epifluorescence microscope, equipped with a 60X plan oil objective and an Andor Ixon EM-CCD camera. Images were processed by Andor IQ software (Adobe, San José, CA, USA). For each time point, at least 100 nuclei were analyzed. The quantitative analysis of the γH2AX foci was performed using ImageJ freeware (NIH; Betheseda, MD, USA) by customised algorithms, as previously described (19).

Flow cytometry analysis and CD45-labeling of lymphocytes. After 2 washings with cold PBS, 10 μl of diluted R-phycoerythrin (1:9 concentration with filtered PBS) coupled to the cyanine dye Cy5 (PECy5)-conjugated mouse anti-human CD45 (leukocyte common antigen, Ly-5) monoclonal antibody (BD Pharmigen, Belgium) were added to each sample and incubated at room temperature for 15 min in the dark. Cells were rinsed and resuspended in 500 μl of cold PBS, and immediately acquired on a flow cytometer (FACSCalibur, BD Biosciences, Belgium), and then, analysed with the CellQuest software (BD Biosciences, Belgium). Lymphocytes were gated based on low side scatter and bright CD45 (BD Pharmigen) staining (20,21) (Fig. 1A and B). Data acquisition was set to analyse 10,000 lymphocytes from a forward scatter (FSC) vs. side scatter (SSC) plot (Fig. 1A). The acquisition gate (region 'Lymphocytes') was set so that only lymphocytes were included for analysis.

γH2AX assay. At 0, 0.25, 1, 2, 4, 6 and 24 h after X-irradiation, PBMCs were washed in PBS, prior to staining with the H2A X phosphorylation assay kit (Millipore, Belgium). PBMCs were fixed in 2% formaldehyde with 0.8% methanol on ice for 20 min, permeabilized with 0.5% saponin, and incubated
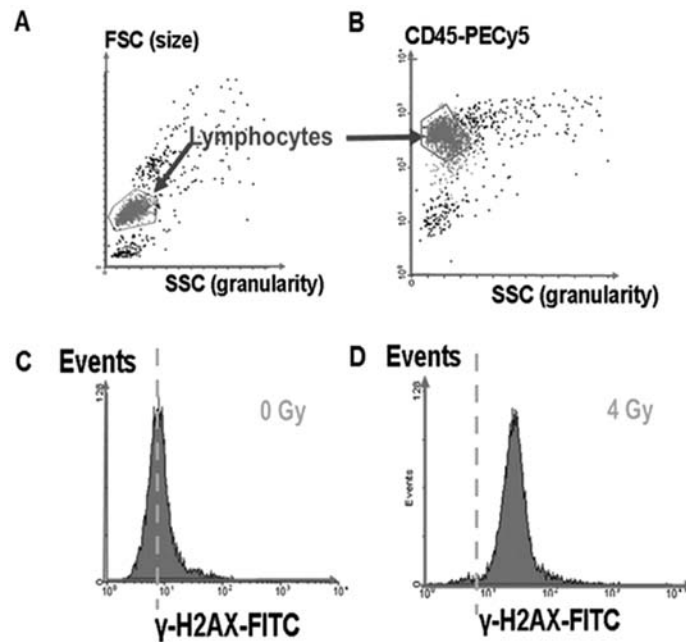
Figure 1. (A) Scatter plot of FSC vs. SSC in which lymphocytes were gated; (B) a representative dot plot of the CD45 expression demonstrating the selection of the lymphocytes. This population was used for further analysis; (C) representative histogram of γH2AX expression in non-irradiated lymphocytes; (D) representative histogram of γH2AX expression in irradiated lymphocytes 30 min after exposure to 4 Gy of X-rays. Note the clear shift in γH2AX expression compared to (C).

on ice for 20 min in the dark with FITC-conjugated mouse monoclonal anti-phospho-histone H2AX, according to the manufacturer's protocol. γH2AX phosphorylation was measured by assessing the level of intracellular fluorescence characterized in lymphocytes, as determined by the mean intensity of the γH2AX positive lymphocytes (Fig. 1C and D).

DNA ladder. PBMCs were collected by centrifugation at different time points after irradiation (0, 4, 24, 48, 72 and 96 h). Genomic DNA samples were isolated by using the high pure PCR template preparation kit (Roche, Belgium). Cells were resuspended in binding buffer and ethanol, and were rinsed prior to the elution of purified DNA. For each sample, the same amount of DNA (200 ng) was loaded on a 1.5% agarose gel containing 0.5 μg/ml ethidium bromide. Electrophoresis was performed at 2 V/cm for 2 h. The DNA in the gels was visualized under ultraviolet light and photographed using a Molecular Imager Gel Doc XR System (Bio-Rad Laboratories, Belgium). The DNA ladder (Fermentas, Belgium) contains bands ranging from 100 to 10,000 bp.

Measurement of the signal intensity on an electrophoresis gel with a DNA ladder was performed using the ImageJ software. All data were expressed as integrated density values (IDV). For each dose, the data from 3 different healthy volunteers were pooled for the determination of the IDV with the error bars representing standard error of the mean (SEM).

TUNEL assay. DNA fragmentation associated with apoptosis was detected by the TdT-mediated dUTP nick end labeling (TUNEL) technique using an *in situ* cell death detection kit (Roche, Belgium). Non-irradiated and irradiated PBMCs were cytospun on coverslips and fixed in 4% paraformaldehyde in PBS after different time points (0, 24, 48, 72 and 96 h). After permeabilization with 0.1% Triton X-100 and 0.1% sodium

citrate (Sigma-Aldrich), cells were incubated at 37°C for 1 h in a humid chamber with TUNEL mixture containing terminal deoxynucleotidyl transferase (TdT) and FITC-dUTP, as recommended by the manufacturer's instructions. Finally, cells were mounted with a mounting medium containing DAPI for DNA counterstaining. The slides were subsequently analyzed by epifluorescence microscopy using an automated Nikon Eclipse Ti microscope equipped with a 20X plan dry objective, and imaged with a Nikon Digital Sight DS-QiMc camera. The images were processed by imaging software NIS-elements (Adobe).

The total number of cells (measured as DAPI+ nuclei) or the number of TUNEL-positive cells in each field was determined. The apoptotic index (% apoptosis) defined as the percentage of TUNEL-positive apoptotic nuclei divided by the number of total cells (DAPI+ nuclei) was quantified with the ImageJ software through customized algorithms. A minimum of 100 nuclei from each condition were counted to generate a mean apoptotic index (AI).

Statistics. All experiments with quantitative analysis included data from at least 3 independent experiments. Data from 3 healthy volunteers were pooled and were expressed as mean ± SEM, and statistical differences ($p < 0.005$) at different doses and times after irradiation were determined with analysis of variance (ANOVA) and the paired t-test.

Results

DSB induction in irradiated lymphocytes analyzed by flow cytometry. The radiation-induced DSBs and repair analysed by flow cytometry in irradiated lymphocytes, is represented in Fig. 2. The error bars in the figure represent the SEM based on the interindividual variation among the 3 donors. A time- and
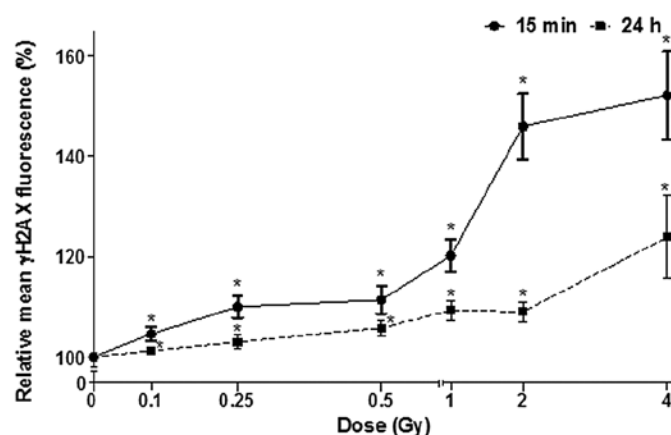
Figure 2. Dose-response curves of lymphocytes from 3 donors analyzed by flow cytometry 15 min and 24 h after X-irradiation. The response curves represent the relative mean γH2AX fluorescence as a function of the irradiation dose. Relative mean of γH2AX fluorescence was calculated by dividing the mean fluorescence of irradiated cells by the mean fluorescence of non-irradiated cells, so that the response at 0 Gy was equal to 100%. Error bars represent ± SEM (n=3). *P<0.05, statistically significant differences in comparison with the control conditions.
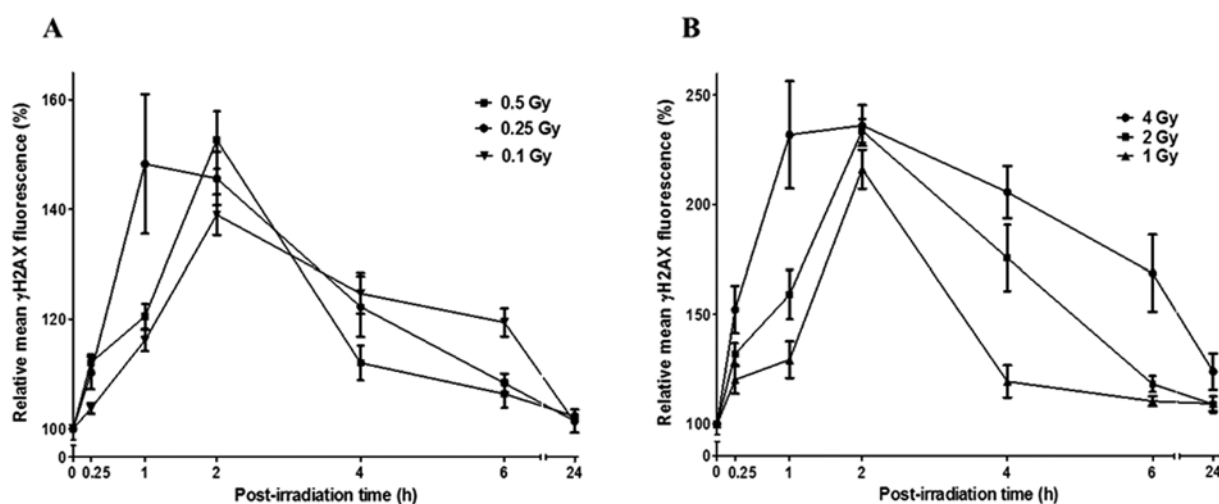

Figure 3. Kinetics of γH2AX formation in lymphocytes after X-irradiation measured by flow cytometry. Relative mean γH2AX fluorescence was calculated by dividing the mean fluorescence of irradiated cells by the mean fluorescence of unirradiated cells, so that the response at 0 Gy was equal to 100%. Time-response curves representing the relative mean fluorescence of γH2AX at different time points after irradiation with (A) low and moderate doses (0.1, 0.25 and 0.5 Gy) or (B) at high doses (1, 2 and 4 Gy). Error bars represent ± SEM (n=3).

dose-dependency in the γH2AX response was shown (two-way ANOVA, P<0.001). An increase in γH2AX phosphorylation was measured 15 min after irradiation. Twenty-four hours after irradiation, a significant decrease of the γH2AX phosphorylation signal due to the subsequent repair in cells was observed (paired t-test, P<0.001). The dose-effect relationship in γH2AX response showed a significant increase in the dose range from 0.1 Gy until 4 Gy (paired t-test, P<0.001). At high doses (1, 2 and 4 Gy), the γH2AX phosphorylation levels were significantly higher compared to low and moderate doses (0.1, 0.25 and 0.5 Gy) for both time points.

Regression analysis was used to fit the data of γH2AX phosphorylation response and showed a dose-linear dependency, slopes being (in %/Gy), 15 min and 24 h after irradiation, respectively, 13.39±2.095 (r^2=0.890, P<0.005) and 5.443±0.6010 (r^2=0.942, P<0.001). For the earlier post-irradiation time (15 min), the dose-response curve in the dose range (0-4 Gy) shows a steeper slope in comparison with the

latter post-irradiation time (24 h) where radiation-induced DSB were mostly repaired.

Kinetics of formation and loss of γH2AX by flow cytometry. Flow cytometry was used to monitor the level of γH2AX in lymphocytes at different time points (0.25, 1, 2, 4, 6, 24 h) after irradiation (0.1, 0.25, 0.5, 1, 2, 4 Gy of X-rays) (Fig. 3). A large interindividual variability in γH2AX levels was observed.

The levels of γH2AX show a time- and dose-dependent response after low and high dose irradiation (two-way ANOVA, P<0.001). The dose-dependency of the γH2AX signal showed a significant difference of γH2AX levels up to 24 h between low/moderate doses (0.1, 0.25 and 0.5 Gy) and high doses (1, 2 and 4 Gy) (paired t-test, P<0.001). The time-course pattern did not differ appreciably among the different individuals for all dose ranges (Fig. 3). A maximum response of γH2AX levels was observed at 1 or 2 h, which was followed by a gradual loss of γH2AX over the next 6 h and a slower
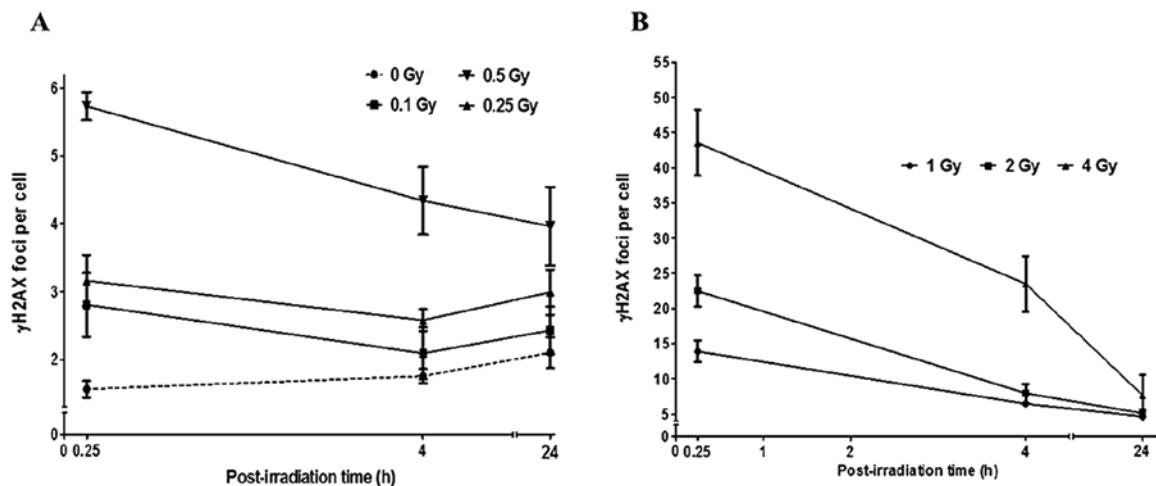
Figure 4. Kinetics of γH2AX foci formation in PBMCs analyzed by fluorescence microscopy. Time response curves represent the relative mean of γH2AX foci at different time points after irradiation. (A) Low and moderate doses (0.1, 0.25 and 0.5 Gy) or (B) high doses (1, 2 and 4 Gy) of X-irradiation. Error bars represent ± SEM (n=3).
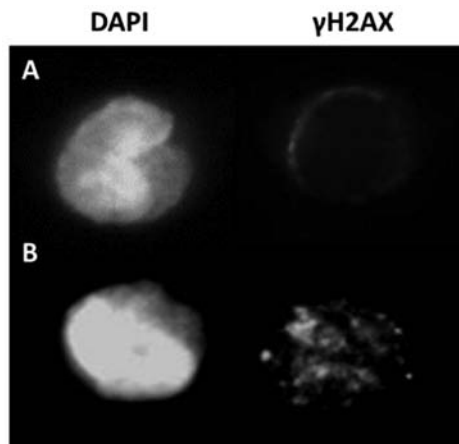

Figure 5. Representative images of PBMCs illustrating γH2AX foci formation, using immunofluorescence microscopy 15 min after X-irradiation. (A) Non-irradiated control; (B) irradiated PBMCs at 4 Gy (nuclei are countertained with DAPI).

decline until 24 h toward background levels (Fig. 3A). At 0.25 and 4 Gy, the maximum response in γH2AX level was maintained for approximately 1 h. The increase and decrease of γH2AX phosphorylation highlights respectively the induction and the subsequent repair of DSBs. After 24 h, the γH2AX signal returned to background levels (Fig. 3A) at all doses, whereas after high doses (1, 2, 4 Gy), the γH2AX levels were significantly higher (Fig. 3B) compared to low doses (0.1, 0.25, 0.5 Gy). Besides a general response, inter individual variations in γH2AX levels were observed at various times following irradiation.

Kinetics of γH2AX formation after X-irradiation. The kinetics of γH2AX foci in PBMCs were analyzed by immunofluorescence microscopy. The presence of radiation-induced γH2AX foci in PBMCs was monitored by immunofluorescence microscopy at different time points (0.25, 1, 2, 4, 6 and 24 h) after irradiation. Immunofluorescence microscopy of γH2AX revealed formation of nuclear foci in PBMCs after

X-irradiation at low, moderate and high doses (0.1, 0.25, 0.5, 1, 2 and 4 Gy) (Figs. 4 and 5). Representative images of γH2AX staining are presented in Fig. 5. For each of the curves, the data from 3 different healthy volunteers were pooled with the error bars representing SEM based on the interindividual variation among the donors.

The number of radiation-induced γH2AX foci showed a significant dose-dependency (two-way ANOVA, P<0.001). The number of γH2AX foci number that was induced 15 min after X-irradiation, was significantly higher (fold-change > 4.5) at high doses (1, 2 and 4 Gy) compared to low and moderate doses (0.1, 0.25 and 0.5 Gy). Time-dependency in radiation-induced γH2AX foci was also shown (two-way ANOVA, P<0.001). Four hours after exposure, a significant decrease in the number of foci per cell was shown at all doses (paired t-test, P<0.001). After 0.1 and 0.25 Gy exposure, the numbers of γH2AX foci per cell returned to background levels (Fig. 4A). However, at 24 h, for doses higher than 0.5 Gy, the number of γH2AX foci per cell was found to be significantly higher than in controls or in cells irradiated at 0.1, 0.25 and 0.5 Gy (Fig. 4B) (paired t-test, P<0.001). Regression analysis did not show a linear dose- or time-dependent relationship in γH2AX foci disappearance (non-significant, P>0.3).

Four hours after irradiation, 74, 81 and 75% respectively, of the initial number of γH2AX foci could still be detected after exposure to 0.1, 0.25 and 0.5 Gy, whereas almost half of the initial number of γH2AX foci disappeared at 1, 2 and 4 Gy, respectively to 46, 35 and 53%. These data show a slower repair of the radiation-induced DSB at low and moderate doses (0.1, 0.25 and 0.5 Gy) in comparison with high doses (1, 2 and 4 Gy). Twenty-four hours after irradiation, 86, 94 and 69% of the initial number of γH2AX foci remained respectively at 0.1, 0.25 and 0.5 Gy whereas at 1, 2 and 4 Gy, respectively, 33, 22 and 17% of the initial number of γH2AX foci were detected. Within 24 h after X-irradiation at low and high doses, the repair is slower than at 4 h and can be explained by the repair of most of the radiation-induced DSBs. The percentages of the initial number of γH2AX foci at 0.1, 0.25 and 0.5 Gy were significantly higher at 24 h compared to 4 h post-irradiation
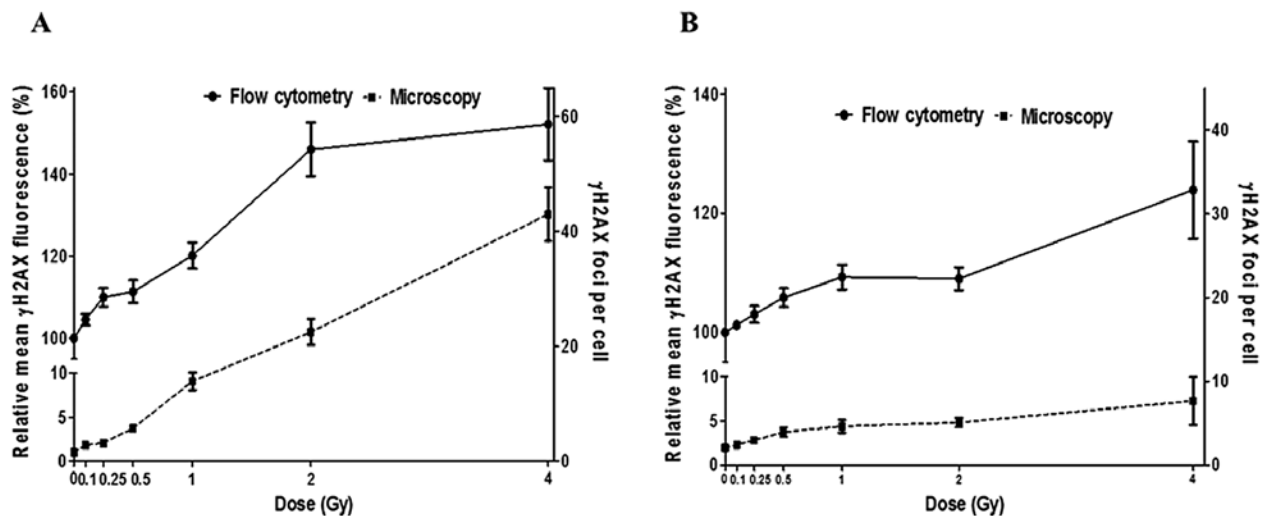
Figure 6. Flow cytometric analysis and microscopic foci analysis for γH2AX measurement (0.1, 0.25, 0.5, 1, 2 and 4 Gy) showing the correlation between the 2 methods at (A) 15 min, and (B) 24 h after irradiation. The experiments were performed in the same 3 donors. The error bars represent ± SEM.
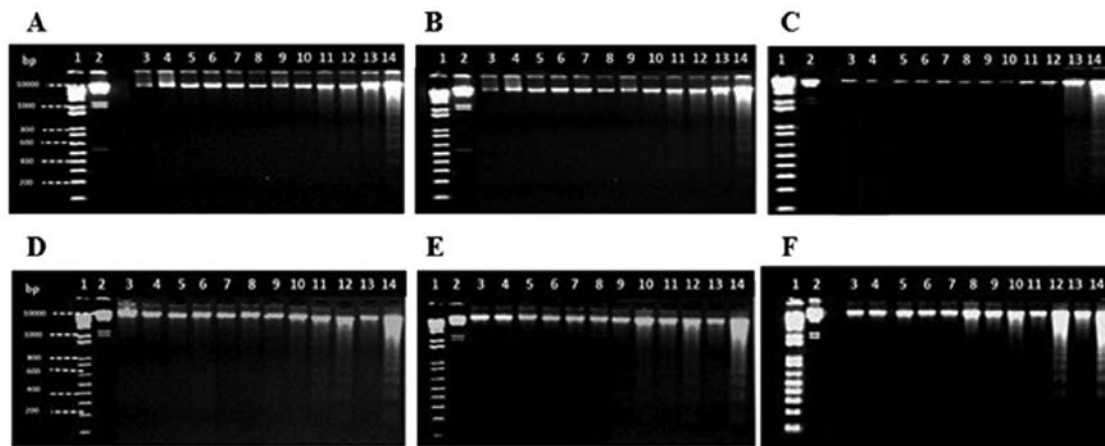

Figure 7. Agarose electrophoresis gel of DNA extracts from PBMCs 0, 4, 24, 48, 72 and 96 h after irradiation, showing DNA internucleosomal fragmentation (A) at 0.1, (B) 0.25, (C) 0.5, (D) 1, (E) 2 and (F) at 4 Gy. Lane 1, 1 kbp ladder marker; lane 2, 10 kbp ladder marker; lane 3, control at 0 h; lane 4, irradiated sample at 0 h; lane 5, control at 4 h; lane 6, irradiated sample at 4 h; lane 7, control at 24 h; lane 8, irradiated sample at 24 h; lane 9, control at 48 h; lane 10, irradiated sample at 48 h; lane 11, control at 72 h; lane 12, irradiated sample at 72 h; lane 13, control at 96 h; lane 14, irradiated sample at 96 h.

due to the low initial foci number. Furthermore, even if most radiation-induced DSBs were repaired 24 h after irradiation, the remaining DSBs were still detectable. The initial number of γH2AX foci at 0.1, 0.25, 0.5, 1, 2 and 4 Gy were significantly higher at 24 h compared to controls.

Correlation between flow cytometry and microscopy. The dose-response curves 15 min and 24 h after X-irradiation obtained by fluorescence microscopy and flow cytometry are presented in Fig. 6. For both methods and time points, the γH2AX response increased in a linear dose-dependent way. The slopes were, in flow cytometry and in microscopy, respectively, at 15 min, 13.39±2.095 (r^2=0.890), 10.46±0.3065 (r^2=0.995), and at 24 h, 5.443±0.6010 (r^2=0.942), 1.289±0.1502 (r^2=0.936) (linear regression, P<0.005). Both methods demonstrated that the slopes decreased within 24 h due to the DSB repair. Fifteen minutes after exposure, we showed a significant increase in γH2AX levels or γH2AX foci number per cell in the different dose ranges. The persistence of γH2AX foci

per cell was further investigated for up to 24 h after radiation exposure (Fig. 6). Residual foci detected 24 h after irradiation were significantly higher at high doses (respectively, from 0.5 to 4 Gy in flow cytometry, and 4 Gy in microscopy, paired t-test, P<0.005). Therefore, γH2AX levels detected by use of flow cytometry in irradiated lymphocytes were consistent with the mean number of microscopically detected γH2AX foci per cell in the same fraction (Fig. 6).

Detection of radiation-induced apoptosis. The nuclease activation of apoptosis can be observed by the formation of a DNA ladder following agarose gel electrophoresis or by labeling of DNA ends (the TUNEL assay) (22), as performed in this study.

DNA ladder. During apoptosis, endonucleases are stimulated and induce genomic DNA fragmentation. These endonucleases are activated by other enzymes called caspases that activate these endonucleases by cutting endonuclease inhibitors. This leads to internucleosomal fragmentation, which leads to the

Table I. Integrated density values (IDV ± SEM, %) based on the DNA ladder electrophoresis performed on PBMCs extracts 48 h after X-irradiation at 0, 0.1, 0.25, 0.5, 1, 2 and 4 Gy.

Bands (bp)	IDV (%), mean ± SEM						
	Control	0.1 Gy	0.25 Gy	0.5 Gy	1 Gy	2 Gy	4 Gy
180	1±0.11	1±0.10	1±0.11	1±0.10	28±0.14	30±0.11	33±0.12
360	1±0.12	1±0.11	1±0.11	1±0.10	33±0.08	32±0.11	35±0.13
540	1±0.09	1±0.10	1±0.11	2±0.10	36±0.11	35±0.12	39±0.12
720	2±0.12	2±0.11	2±0.12	2±0.12	38±0.12	39±0.12	44±0.09
900	2±0.09	2±0.12	2±0.11	2±0.12	41±0.06	43±0.08	49±0.08

Table II. Integrated density values (IDV ± SEM, %) based on DNA ladder electrophoresis performed on PBMC extracts 96 h after X-irradiation at 0, 0.1, 0.25, 0.5, 1, 2 and 4 Gy.

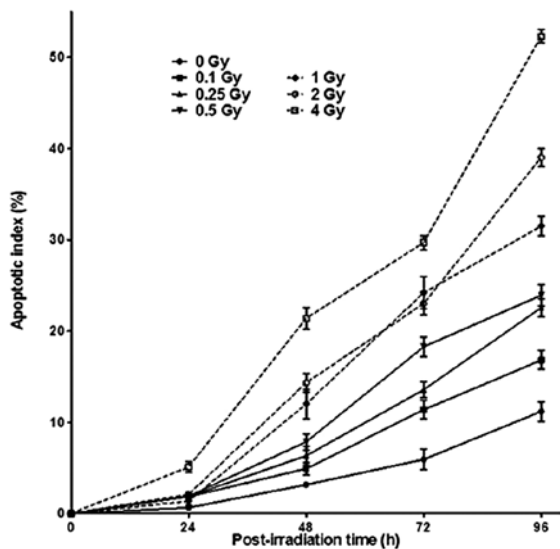| Bands (bp)	IDV (%), mean ± SEM						
	Control	0.1 Gy	0.25 Gy	0.5 Gy	1 Gy	2 Gy	4 Gy
180	19±0.11	23±0.14	26±0.13	29±0.11	34±0.12	35±0.12	46±0.13
360	22±0.12	32±0.08	33±0.1	36±0.11	42±0.13	44±0.1	56±0.11
540	30±0.09	38±0.11	39±0.11	41±0.12	46±0.12	48±0.13	64±0.09
720	36±0.12	41±0.12	44±0.09	46±0.12	48±0.09	49±0.1	70±0.1
900	39±0.09	49±0.06	49±0.1	50±0.08	55±0.08	55±0.1	71±0.11

Figure 8. Spontaneous and radiation-induced apoptosis in PBMCs 0, 24, 48, 72 and 96 h after irradiation at low, moderate and high doses (0.1, 0.25, 0.5, 1, 2 and 4 Gy). The apoptotic index (AI) was used to represent radiation-induced levels of apoptosis at different time points after X-irradiation. The error bars represent ± SEM (n=3).

formation of mono- (180 bp) and oligonucleosomes. This process can be visualized through the appearance of a 'DNA ladder' by a gel electrophoresis technique. Radiation-induced apoptosis in PBMCs was analyzed for the presence of the DNA ladder at different time points (0, 24, 48, 72 and 96 h) after low and high dose X-irradiation (0.1, 0.25, 0.5, 1, 2 and

4 Gy) (Fig. 7). In addition, although DNA ladder gel electrophoresis is a semi-quantitative method for DNA fragmentation in apoptosis, the apoptotic fragmentation was evaluated with the IDV (Tables I and II). We showed that the apoptotic DNA fragmentation increased significantly depending on the dose (paired t-test, P<0.005). Indeed, after irradiation with low and moderate doses (0.1, 0.25 and 0.5 Gy), an increase in DNA fragmentation was observed only after 96 h (Table I). At high doses (1, 2 and 4 Gy), an increase in DNA fragmentation was clearly observed already from 48 h onwards after irradiation. We also showed that at high doses (1, 2 and 4 Gy) there was a significant time-dependent increase in DNA fragmentation between 48 h (a beginning of genomic DNA fragmentation was observed) and 96 h (Tables I and II). At 72 and 96 h, apoptotic DNA fragmentation was clearly observed and the band intensity increased significantly after irradiation (P< 0.005).

TUNEL assay. Levels of spontaneous or radiation-induced apoptosis in PBMCs samples are presented in Fig. 8 after different incubation times (0, 24, 48, 72 and 96 h) with different doses of X-rays (0, 0.1, 0.25, 0.5, 1, 2 and 4 Gy). The apoptotic index was used to represent radiation-induced levels of apoptosis. Representative images of PBMCs analysed by a TUNEL assay are illustrated in Fig. 9.

Using the TUNEL assay, DNA fragmentation was detected at the early time points (starting from 24 h in all dose ranges, Fig. 8). Indeed, early in the process of apoptosis, DNA cleavage generates high molecular weight (HMW) fragments which can be detected by the TUNEL assay. This is followed by a pronounced DNA breakdown into low molecular weight (LMW) fragments, detected as a 'DNA ladder' by
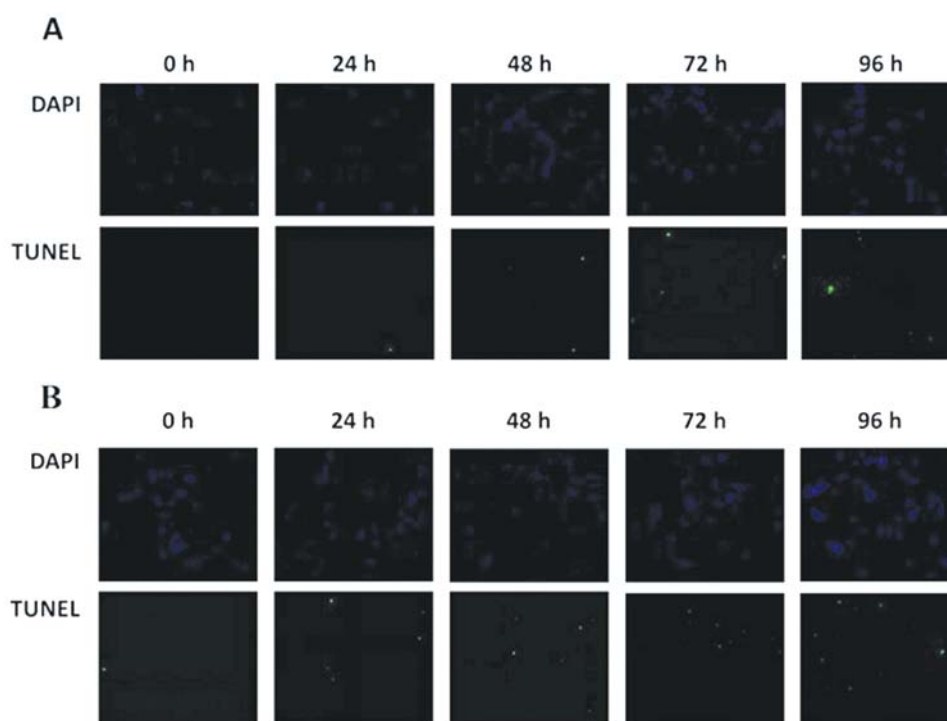
Figure 9. A gallery of images of PBMCs, using the TUNEL assay analyzed by microscopy, illustrating the DNA fragmentation at different time points (0, 24, 48, 72 and 96 h) (A) in controls or (B) in irradiated samples at 0.1 Gy (nuclei were counterstained with DAPI).

conventional agarose gel electrophoresis (mono-, 180-bp and oligonucleosomes). The TUNEL assay is considered as a more sensitive method (from 24 h in all dose ranges, Fig. 8) for detection of apoptosis compared to DNA ladder gel electrophoresis. By DNA ladder, the apoptotic DNA fragmentation was detected respectively, starting at 48 h at high doses (1, 2, and 4 Gy) and at only 96 h after low/moderate doses of X-rays (0.1, 0.25, 0.5 Gy).

Using the TUNEL assay, we observed spontaneous apoptosis in non-irradiated controls, as well as radiation-induced apoptosis after 24 until 96 h post-irradiation. In this time course, the level of spontaneous apoptosis was significantly lower compared to radiation-induced apoptosis.

The results obtained from the TUNEL assay showed a time- and dose-dependency in radiation-induced apoptosis (two-way ANOVA, P<0.005).

Regression analysis (P<0.005) was used and showed a time-linear dependency, slopes being at 0.1, 0.25, 0.5, 1, 2 and 4 Gy, respectively, 0.18±0.022 (r^2=0.935), 0.24±0.034 (r^2=0.939), 0.27±0.033 (r^2=0.955), 0.36±0.043 (r^2=0.957), 0.41±0.054 (r^2=0.950), 0.53±0.067, (r^2=0.955). These data showed a significant increase of the slope in the apoptotic response from 0.1 until 4 Gy of X-ray irradiation (with a maximum apoptotic index at 96 h).

Discussion

Kinetics of DSB foci formation using microscopy. One of the earliest stages in the cellular response to DSBs is the phosphorylation of the histone variant H2AX. Discrete nuclear foci at sites of DSBs can be visualized by immunofluorescence microscopy (6). In our *in vitro* experiments, we found a linear dose-dependent response in γH2AX foci formation in irradi-

ated PBMCs. The number of γH2AX foci linearly increased with the radiation dose studied (0-4 Gy). In PBMCs fixed 15 min after exposure to ionizing radiation, we measured on average 2.8 (±0.47) foci/cell/Gy at 0.1 Gy compared to 3 foci/cell estimated and reported in irradiated whole blood cells and T-lymphocytes at 0.1 Gy (23). These results show a general agreement among different investigators. Similarly, we measured on average 5.7 (±0.20) and 13.9 (±1.52) foci/cell at respective doses of 0.5 and 1 Gy while Rothkamm *et al* (24) reported in irradiated PBMCs 5.5 and 11.5 foci/cell for the same dose. The estimation of 13.9 (±1.52) foci/cell after 1 Gy irradiation is a rather low number compared to estimates usually seen with cells in culture such as lymphoblastoid cells (25,26), human fibroblast cells (27) or human breast cancer cells (28). The lower number of γH2AX foci in PBMCs could have several explanations. First, G0 cells possess less genetic material than dividing cells in culture. In fact, a previous study (26) showed that twice as many γH2AX foci are observed in metaphase cells relative to G1 cells at any given dose. Second, it is known that higher order chromatin structure can also influence the distribution of DNA DSBs. For example, in higher eukaryotic cells, some part of chromatin is condensed to make heterochromatin which is refractory to γH2AX foci formation (29). The differences observed could be due to various technical issues and/or variations in foci counting by different investigators.

Furthermore, we showed a time-dependent induction and disappearance in γH2AX focus formation. The formation of γH2AX foci at the DNA damage site is fast, with γH2AX foci forming within 3-15 min and reaching a maximum level followed by a dephosphorylation over the next few hours (6,9,30-33). *In vitro* studies on irradiated human lymphocytes found a maximum level of γH2AX foci within 15-30 min

(34-36), in agreement with our results. For cell cultures, 30 min is found to be the optimum time for determining the maximum yield of H2AX foci for various cell types such as human lung embryonic fibroblasts, human fetal lung fibroblasts and human breast tumor cell line (6,31,37). In the time-course, we showed that DNA DSBs are repaired with biphasic kinetics, a rapid phase lasting several hours (a rapid decline in γH2AX foci until 4 h) followed by a slower phase (a slower loss of γH2AX foci until 24 h). This DSB repair kinetic pattern has been reported previously by Sedelnikova *et al* (33), in human peripheral blood lymphocytes and in human fibroblasts after γ-irradiation. These kinetics can be explained by the fact that ionizing radiation induces DSBs that can vary from simple to more complex structures (38,39). For low-linear energy transfer (LET) radiation, it has been estimated that 20-40% of the initial damage is complex (38-40). We can hypothesize that this non-uniformity in DNA damage would result in a delay in the repair of the more complex DSBs. Multiple high number of adjacent DSBs could inhibit the attachment of repair proteins to other nearby DSBs, and this possibility increases with the ionization density or LET of the radiation (32). The slow component of DSB repair (after 4 h) would be consistent with the accumulation of repair factors in the foci. Indeed, the time course of localization of various proteins in the foci indicates that they are assembled in a defined sequence. Mediator of DNA damage checkpoint protein 1 (MDC1) and p53 binding protein 1 (53BP1) colocalize very rapidly 5-15 min after irradiation (41,42). MDC1 plays an important role in assembling other repair and checkpoint proteins (43). A previous study (44) indicates that the interacting MDC1 and γH2AX molecules form an 'affinity platform' on which other proteins are assembled and retained (12,42). As discussed previously (45), modification of the H2AX molecules may be important to alter the local chromatin structure in the surrounding of a DSB thereby increasing the accessibility of DNA to various repair factors.

In the present study, the immunofluorescence-based assay that allows the visualization of discrete nuclear foci formed as a result of H2AX phosphorylation was shown to be a sensitive and reliable method for detecting radiation-induced DSBs. Our results indicate that γH2AX foci may be a quantitative biomarker of human radiation exposure. Given its specificity and sensitivity, analysis of γH2AX foci can be also a useful method of investigating DNA damage and repair efficiency.

Linear dose-response in radiation-induced H2AX phosphorylation using flow cytometry. Currently, the γH2AX focus formation is being used as a DNA damage marker, specifically for DSBs induced by exposure to various genotoxic agents, such as ionizing radiation (6). In this study, we thought that by measuring cellular levels of γH2AX by high-throughput flow cytometry will allow straightforward assessments of radiation-induced DNA damage and ability to repair such DNA damage.

Using flow cytometric analysis, the dose response of γH2AX induction in lymphocytes was found to be linear in the studied dose range (0-4 Gy). These results are similar to the results we obtained by γH2AX foci formation analyzed by immufluorescence microscopy. This is in agreement with previous studies using mainly microscopy that showed a linear dose response up to 40 Gy with a gradual saturation above this dose (5,6,8,9,46-49). By examining the time course of the γH2AX response, our results showed that the intensity of the γH2AX signal increased rapidly up to 1 h. A maximum response was observed between 1 and 2 h and was maintained for approximately 1 h (as seen at 0.25 and 4 Gy) before starting to decrease towards background levels. This time point of maximum response is different than in microscopy: the γ-H2AX quantification in flow cytometry is based on measuring the total fluorescence intensity for each cell while fluorescence microscopy imaging is depend on γ-H2AX foci scoring. By 24 h, the γH2AX signal had returned to background levels at all doses except at 4 Gy due to DSB repair. Similar results have been reported in other studies, with H2AX phosphorylation being detected as soon as 1-3 min post irradiation and the maximum response at 9-30 min (5,6,31,48,49). In agreement with our study, previous studies using human lymphocytes found maximum γH2AX induction at 1-2 h post-exposure (50). All of these previous studies support the idea that the exact form of time response depends on the dose and the type of cells, although irradiation conditions (temperature) (51) could also have an effect on the response time (8,9,48,49). This supports previous findings that radioresistant cultures dephosphorylate faster than radiosensitive ones (8,9,49,52). In our study, the half-time of H2AX dephosphorylation was estimated from the time response curves and found to be 2-4 h which is in agreement with a previous study (3 h, in human peripheral blood lymphocytes) (30).

This flow cytometry assay has been used to characterize the radiation response of lymphocytes. Flow cytometry is a rapid tool for measuring the induction of DNA DSB damage, although the total signal measured does not provide the same level of sensitivity as counting the number and/or size of the γH2AX foci by microscopy. Furthermore, the ability of flow cytometers to analyze thousands of lymphocytes every second allows the reduction of processing times from days to hours, working with multiple samples simultaneously. In contrast, the immunofluorescence microscopy-based assay is time-consuming, operator-dependent and is not easily scalable for high throughput assay development. In this study, results showed a linear response with the dose in γH2AX phosphorylation by flow cytometry. These findings reinforce the idea that γH2AX biodosimetry can be a robust tool for estimating radiation exposure. This flow cytometry based method can be used on a large scale to assess its potential as rapid, high throughput biodosimeter for mass casualty situations.

Residual foci and radiation-induced apoptosis. The majority of DSBs are repaired within a few hours post-irradiation. Localization of DSB in specific areas of chromatin or complexity of DSB may be important constraints for the efficiency of the DSB repair. In this context, DSB present in residual foci (representing unrepaired DNA damage) may hypothetically represent a sufficient event for triggering apoptosis.

Induction of apoptosis in human lymphocytes and subpopulations of human lymphocytes (53) by ionizing radiation has been observed both *in vitro* (54,55) and *in vivo* (56). DNA damage results in a coordinated network of signal transduction pathways involved in cell cycle arrest, apoptosis, stress response and activation of the DNA repair processes (57). In

our study, differences were observed in the ability of PBMCs to repair DSBs induced by X-rays in the studied dose range. At 24 h after irradiation, the lower numbers of DSBs induced by lower doses (0.1 and 0.25 Gy) of radiation were repaired more easily than the large number of DSBs induced by the higher doses (0.5, 1, 2 and 4 Gy). According to the data obtained, after the higher doses a large number of unrepaired ionizing radiation-induced foci persisted in cells 24 h after irradiation. However, so far, no data are available to correlate residual DSB with radiation-induced apoptosis in lymphocytes. DSB in residual foci may represent a sufficient event for triggering apoptosis. Localization of DSB in specific areas of chromatin or complexity of DSB may be important constraints for the efficiency of the DSB repair. In particular, 2 or more DSBs might be involved in the formation of residual foci. Such breaks may take a longer time to be repaired and could result in triggering the apoptotic signal transduction because of the failure to repair DSBs.

Other radiation-induced foci may contain only 1, or less complex DSB, which may be subjected to faster repair and therefore do not signal for apoptosis. Radiation-induced unrepaired DSBs may be responsible for the induction of apoptosis. In our study, we showed by DNA ladder gel electrophoresis that the highest level of apoptotic fragmentation was observed after 96 h at low and moderate doses (0.1, 0.25, 0.5 Gy) and after 48 h at high doses (1, 2 and 4 Gy). It should be noted that the kinetics of apoptosis induced by irradiation *in vivo* may be different from that found after irradiation of cells *in vitro*. Apoptosis *in vivo* is already observed after 3-12 h following irradiation (58-61), while apoptosis *in vitro* requires 24-48 h to reach maximal levels (54,62,63). The TUNEL assay results revealed that the frequency of apoptotic cells progressively increased in a dose- and time-dependent manner. The DNA cleavage into large fragments detected by the sensitive TUNEL assay is an early event observed in the apoptotic cascade before the typical endonuclease cleavage into 180 to 200 bp can be detected as a 'DNA ladder' (64). This DNA breakage is exactly what we observed in our experiments. DNA damage monitoring and signaling processes are responsible for cell cycle checkpoint control and failure of these checkpoints leads to cell death (65). The key players in DNA damage recognition and signaling are p53, DNA-PK, poly(ADP ribose) polymerase (PARP), and ATM. PARP, DNA-PK and ATM act upstream of p53. Previous studies (66-68) have suggested that DNA-PK plays a pivotal role in apoptosis. The cell cycle arrest induced by DNA damage may result in DNA repair and therefore in removal of the cell cycle blockade, when the repair is completed. If, however, cells undergo apoptosis, their capacity to repair damaged DNA is suppressed as enzymes responsible for DNA damage repair are cleaved by proteases (67). In apoptosis, nuclear chromatin undergoes condensation, during which a calcium-dependent endonuclease is activated, resulting in cleavage of nuclear DNA into fragments of 180-200 base pairs in length or multiples of them (69,70). Induction of apoptosis in human lymphocytes and subpopulations of human lymphocytes (53) by ionizing radiation has been observed both *in vitro* (54,55) and *in vivo* (56). It is important to note that some cell types are more sensitive to undergo apoptosis than others and that the signaling pathways employed by these different cell types

to induce apoptosis may vary accordingly. Radiation-induced apoptotic signaling can be initiated in different cellular compartments, including the nucleus, cytosolic elements and plasma membrane.

In this study, we showed the cytotoxic effects of radiation in irradiated PBMCs from healthy donors by measurement of apoptosis. These adverse biological effects induced by radiation in terms of cytotoxicity is important for acute effects because apoptosis is a rapid process that can dramatically reduce cell number. Furthermore, a dose- and time-dependency of apoptotic fragmentation in irradiated cells can be used as a marker to predict unusual risk of side effects, to diagnose a cytotoxicity as radiation-related, and in the case of bioterror, allow for tissue-specific biodosimetry.

In conclusion, H2AX has been widely used by many researchers as a tool to measure radiation-induced DNA damage. In the present study, a linear dose-dependency of γH2AX phosphorylation was observed in γH2AX foci in PBMCs detected by microscopy as well as measured by flow cytometry from 15 min until 24 h following irradiation. These findings showed that γH2AX itself is a good candidate for biodosimetry. In addition, our results show the exciting opportunity to employ γH2AX foci formation for monitoring human exposure to low doses (<100 mGy) of ionizing radiation. Furthermore, PBMCs are easily obtained with minimal invasion, have very low levels of background γH2AX expression validating its use as a tissue sample for damage detection following radiation exposure (24,48,49). The use of γH2AX as a high throughput biodosimeter in flow cytometry would be useful for a day post-exposure applications, like large-scale radiological events or radiation therapy.

Of the different types of radiation-induced deleterious cellular lesions, DSBs have been considered to be the most relevant for cytotoxic effects of radiation and induction of apoptosis (71,72). In our study, we explored the association between radiation-induced DNA damage, estimated by the number of DSB induced in the studied radiation dose (0-4 Gy) and the radiation-induced apoptosis rates. Radiation-induced apoptosis could be a biodosimetric indicator in the case of radiation exposure.

After 24 h, residual γH2AX foci were still detectable in irradiated cells, and apoptotic fragmentation was observed from 24 until 96 h in a dose-dependent manner. Modulation of the apoptotic response, which might be explained by the inefficiency or misrepair of the DSBs, can result in transduction pathways enhancing the cytotoxic effect of radiation. These signal transduction pathways include the radiation-induced apoptosis. Which of these signaling systems is instrumental for apoptosis induction is still unknown and may depend on the cell system, the type of stimulus and the input of other apoptosis-regulating factors.

Acknowledgements

References

1. Bakkenist CJ and Kastan MB: DNA damage activates ATM through intermolecular autophosphorylation and dimer dissociation. Nature 421: 499-506, 2003.
2. Bartek J and Lukas J: DNA repair: damage alert. Nature 421: 486-488, 2003.
3. Hoeijmakers JH: Genome maintenance mechanisms for preventing cancer. Nature 411: 366-374, 2001.
4. Shiloh Y: ATM and related protein kinases: safeguarding genome integrity. Nat Rev Cancer 3: 155-168, 2003.
5. Rogakou EP, Pilch DR, Orr AH, Ivanova VS and Bonner WM: DNA double-stranded breaks induce histone H2AX phosphorylation on serine 139. J Biol Chem 273: 5858-5868, 1998.
6. Rogakou EP, Boon C, Redon C and Bonner WM: Megabase chromatin domains involved in DNA double-strand breaks in vivo. J Cell Biol 146: 905-916, 1999.
7. Kuerbitz SJ, Plunkett BS, Walsh WV and Kastan MB: Wild-type p53 is a cell cycle checkpoint determinant following irradiation. Proc Natl Acad Sci USA 89: 7491-7495, 1992.
8. MacPhail SH, Banath JP, Yu TY, Chu EH, Lambur H and Olive PL: Expression of phosphorylated histone H2AX in cultured cell lines following exposure to X-rays. Int J Radiat Biol 79: 351-358, 2003.
9. Banath JP, Macphail SH and Olive PL: Radiation sensitivity, H2AX phosphorylation, and kinetics of repair of DNA strand breaks in irradiated cervical cancer cell lines. Cancer Res 64: 7144-7149, 2004.
10. Fernandez-Capetillo O, Lee A, Nussenzweig M and Nussenzweig A: H2AX: the histone guardian of the genome. DNA Repair (Amst) 3: 959-967, 2004.
11. Lukas C, Falck J, Bartkova J, Bartek J and Lukas J: Distinct spatiotemporal dynamics of mammalian checkpoint regulators induced by DNA damage. Nat Cell Biol 5: 255-260, 2003.
12. Lukas C, Melander F, Stucki M, et al: Mdc1 couples DNA double-strand break recognition by Nbs1 with its H2AX-dependent chromatin retention. EMBO J 23: 2674-2683, 2004.
13. Mailand N, Bekker-Jensen S, Faustrup H, et al: RNF8 ubiquitylates histones at DNA double-strand breaks and promotes assembly of repair proteins. Cell 131: 887-900, 2007.
14. Bekker-Jensen S, Lukas C, Kitagawa R, et al: Spatial organization of the mammalian genome surveillance machinery in response to DNA strand breaks. J Cell Biol 173: 195-206, 2006.
15. Su TT: Cellular responses to DNA damage: one signal, multiple choices. Annu Rev Genet 40: 187-208, 2006.
16. Story MD, Voehringer DW, Malone CG, Hobbs ML and Meyn RE: Radiation-induced apoptosis in sensitive and resistant cells isolated from a mouse lymphoma. Int J Radiat Biol 66: 659-668, 1994.
17. Bennett CB, Lewis AL, Baldwin KK and Resnick MA: Lethality induced by a single site-specific double-strand break in a dispensable yeast plasmid. Proc Natl Acad Sci USA 90: 5613-5617, 1993.
18. Huang X, Okafuji M, Traganos F, Luther E, Holden E and Darzynkiewicz Z: Assessment of histone H2AX phosphorylation induced by DNA topoisomerase I and II inhibitors topotecan and mitoxantrone and by the DNA cross-linking agent cisplatin. Cytometry A 58: 99-110, 2004.
19. De Vos WH, Van Neste L, Dieriks B, Joss GH and Van Oostveldt P: High content image cytometry in the context of subnuclear organization. Cytometry A 77: 64-75, 2010.
20. Schnizlein-Bick CT, Mandy FF, O'Gorman MR, et al: Use of CD45 gating in three and four-color flow cytometric immunophenotyping: guideline from the National Institute of Allergy and Infectious Diseases, Division of AIDS. Cytometry 50: 46-52, 2002.
21. Glencross D, Scott LE, Jani IV, Barnett D and Janossy G: CD45-assisted PanLeucogating for accurate, cost-effective dual-platform CD4+ T-cell enumeration. Cytometry 50: 69-77, 2002.
22. Darzynkiewicz Z and Traganos F: Measurement of apoptosis. Adv Biochem Eng Biotechnol 62: 33-73, 1998.
23. Beels L, Werbrouck J and Thierens H: Dose response and repair kinetics of gamma-H2AX foci induced by in vitro irradiation of whole blood and T-lymphocytes with X- and gamma-radiation. Int J Radiat Biol 86: 760-768, 2010.
24. Rothkamm K, Balroop S, Shekhdar J, Fernie P and Goh V: Leukocyte DNA damage after multi-detector row CT: a quantitative biomarker of low-level radiation exposure. Radiology 242: 244-251, 2007.
25. Kato TA, Nagasawa H, Weil MM, Little JB and Bedford JS: Levels of gamma-H2AX Foci after low-dose-rate irradiation reveal a DNA DSB rejoining defect in cells from human ATM heterozygotes in two at families and in another apparently normal individual. Radiat Res 166: 443-453, 2006.
26. Kato TA, Okayasu R and Bedford JS: Comparison of the induction and disappearance of DNA double strand breaks and gamma-H2AX foci after irradiation of chromosomes in G1-phase or in condensed metaphase cells. Mutat Res 639: 108-112, 2008.
27. Leatherbarrow EL, Harper JV, Cucinotta FA and O'Neill P: Induction and quantification of gamma-H2AX foci following low and high LET-irradiation. Int J Radiat Biol 82: 111-118, 2006.
28. Yasui LS: GammaH2AX foci induced by gamma rays and ^{125}IdU decay. Int J Radiat Biol 80: 895-903, 2004.
29. Goodarzi AA, Noon AT, Deckbar D, et al: ATM signaling facilitates repair of DNA double-strand breaks associated with heterochromatin. Mol Cell 31: 167-177, 2008.
30. Olive PL and Banath JP: Phosphorylation of histone H2AX as a measure of radiosensitivity. Int J Radiat Oncol Biol Phys 58: 331-335, 2004.
31. Antonelli F, Belli M, Cuttone G, et al: Induction and repair of DNA double-strand breaks in human cells: dephosphorylation of histone H2AX and its inhibition by calyculin A. Radiat Res 164: 514-517, 2005.
32. Cucinotta FA, Pluth JM, Anderson JA, Harper JV and O'Neill P: Biochemical kinetics model of DSB repair and induction of gamma-H2AX foci by non-homologous end joining. Radiat Res 169: 214-222, 2008.
33. Sedelnikova OA, Horikawa I, Redon C, et al: Delayed kinetics of DNA double-strand break processing in normal and pathological aging. Aging Cell 7: 89-100, 2008.
34. Sak A and Stuschke M: Use of gammaH2AX and other biomarkers of double-strand breaks during radiotherapy. Semin Radiat Oncol 20: 223-231, 2010.
35. Redon CE, Dickey JS, Bonner WM and Sedelnikova OA: Gamma-H2AX as a biomarker of DNA damage induced by ionizing radiation in human peripheral blood lymphocytes and artificial skin. Adv Space Res 43: 1171-1178, 2009.
36. Roch-Lefevre S, Mandina T, Voisin P, et al: Quantification of gamma-H2AX foci in human lymphocytes: a method for biological dosimetry after ionizing radiation exposure. Radiat Res 174: 185-194, 2010.
37. Paull TT, Rogakou EP, Yamazaki V, Kirchgessner CU, Gellert M and Bonner WM: A critical role for histone H2AX in recruitment of repair factors to nuclear foci after DNA damage. Curr Biol 10: 886-895, 2000.
38. Goodhead DT: Initial events in the cellular effects of ionizing radiations: clustered damage in DNA. Int J Radiat Biol 65: 7-17, 1994.
39. Nikjoo H, O'Neill P, Wilson WE and Goodhead DT: Computational approach for determining the spectrum of DNA damage induced by ionizing radiation. Radiat Res 156: 577-583, 2001.
40. Gulston M, Fulford J, Jenner T, de Lara C and O'Neill P: Clustered DNA damage induced by gamma radiation in human fibroblasts (HF19), hamster (V79-4) cells and plasmid DNA is revealed as Fpg and Nth sensitive sites. Nucleic Acids Res 30: 3464-3472, 2002.
41. Schultz LB, Chehab NH, Malikzay A and Halazonetis TD: p53 binding protein 1 (53BP1) is an early participant in the cellular response to DNA double-strand breaks. J Cell Biol 151: 1381-1390, 2000.
42. Stucki M, Clapperton JA, Mohammad D, Yaffe MB, Smerdon SJ and Jackson SP: MDC1 directly binds phosphorylated histone H2AX to regulate cellular responses to DNA double-strand breaks. Cell 123: 1213-1226, 2005.
43. Xu X and Stern DF: NFBD1/MDC1 regulates ionizing radiation-induced focus formation by DNA checkpoint signaling and repair factors. FASEB J 17: 1842-1848, 2003.
44. Stucki M and Jackson SP: gammaH2AX and MDC1: anchoring the DNA-damage-response machinery to broken chromosomes. DNA Repair (Amst) 5: 534-543, 2006.
45. Paull TT and Gellert M: The 3' to 5' exonuclease activity of Mre11 facilitates repair of DNA double-strand breaks. Mol Cell 1: 969-979, 1998.
46. Bonner WM: Low-dose radiation: thresholds, bystander effects, and adaptive responses. Proc Natl Acad Sci USA 100: 4973-4975, 2003.
47. Pilch DR, Sedelnikova OA, Redon C, Celeste A, Nussenzweig A and Bonner WM: Characteristics of gamma-H2AX foci at DNA double-strand breaks sites. Biochem Cell Biol 81: 123-129, 2003.
48. Rothkamm K and Lobrich M: Evidence for a lack of DNA double-strand break repair in human cells exposed to very low x-ray doses. Proc Natl Acad Sci USA 100: 5057-5062, 2003.

49. Lobrich M, Rief N, Kuhne M, *et al*: In vivo formation and repair of DNA double-strand breaks after computed tomography examinations. Proc Natl Acad Sci USA 102: 8984-8989, 2005.
50. Hamasaki K, Imai K, Nakachi K, Takahashi N, Komada Y and Kusunoki Y: Short-term culture and gammaH2AX flow cytometry determine differences in individual radiosensitivity in human peripheral T lymphocytes. Environ Mol Mutagen 48: 38-47, 2007.
51. Hamada N, Schettino G, Kashino G, *et al*: Histone H2AX phosphorylation in normal human cells irradiated with focused ultrasoft X rays: evidence for chromatin movement during repair. Radiat Res 166: 31-38, 2006.
52. Taneja N, Davis M, Choy JS, *et al*: Histone H2AX phosphorylation as a predictor of radiosensitivity and target for radiotherapy. J Biol Chem 279: 2273-2280, 2004.
53. Ozsahin M, Ozsahin H, Shi Y, Larsson B, Wurgler FE and Crompton NE: Rapid assay of intrinsic radiosensitivity based on apoptosis in human CD4 and CD8 T-lymphocytes. Int J Radiat Oncol Biol Phys 38: 429-440, 1997.
54. Boreham DR, Gale KL, Maves SR, Walker JA and Morrison DP: Radiation-induced apoptosis in human lymphocytes: potential as a biological dosimeter. Health Phys 71: 685-691, 1996.
55. Hertveldt K, Philippe J, Thierens H, Cornelissen M, Vral A and De Ridder L: Flow cytometry as a quantitative and sensitive method to evaluate low dose radiation induced apoptosis in vitro in human peripheral blood lymphocytes. Int J Radiat Biol 71: 429-433, 1997.
56. Delic J, Magdelenat H, Barbaroux C, *et al*: In vivo induction of apoptosis in human lymphocytes by therapeutic fractionated total body irradiation. Br J Radiol 68: 997-1003, 1995.
57. Kanaar R, Hoeijmakers JH and van Gent DC: Molecular mechanisms of DNA double strand break repair. Trends Cell Biol 8: 483-489, 1998.
58. Ijiri K and Potten CS: The circadian rhythm for the number and sensitivity of radiation-induced apoptosis in the crypts of mouse small intestine. Int J Radiat Biol 58: 165-175, 1990.
59. Stephens LC, Ang KK, Schultheiss TE, Milas L and Meyn RE: Apoptosis in irradiated murine tumors. Radiat Res 127: 308-316, 1991.
60. Inouye M, Tamaru M and Kameyama Y: Effects of cycloheximide and actinomycin D on radiation-induced apoptotic cell death in the developing mouse cerebellum. Int J Radiat Biol 61: 669-674, 1992.
61. Palayoor ST, Macklis RM, Bump EA and Coleman CN: Modulation of radiation-induced apoptosis and G2/M block in murine T-lymphoma cells. Radiat Res 141: 235-243, 1995.
62. Ling CC, Chen CH and Li WX: Apoptosis induced at different dose rates: implication for the shoulder region of cell survival curves. Radiother Oncol 32: 129-136, 1994.
63. Abend M, Rhein A, Gilbertz KP, Blakely WF and Van Beuningen D: Correlation of micronucleus and apoptosis assays with reproductive cell death. Int J Radiat Biol 67: 315-326, 1995.
64. Brown DG, Sun XM and Cohen GM: Dexamethasone-induced apoptosis involves cleavage of DNA to large fragments prior to internucleosomal fragmentation. J Biol Chem 268: 3037-3039, 1993.
65. Elledge SJ: Cell cycle checkpoints: preventing an identity crisis. Science 274: 1664-1672, 1996.
66. Candeias SM, Durum SK and Muegge K: p53-dependent apoptosis and transcription of p21waf/cip1/sdi1 in SCID mice following gamma-irradiation. Biochimie 79: 607-612, 1997.
67. Mountz JD, Wu J, Zhou T and Hsu HC: Cell death and longevity: implications of Fas-mediated apoptosis in T-cell senescence. Immunol Rev 160: 19-30, 1997.
68. Song Q, Burrows SR, Smith G, *et al*: Interleukin-1 beta-converting enzyme-like protease cleaves DNA-dependent protein kinase in cytotoxic T cell killing. J Exp Med 184: 619-626, 1996.
69. Wyllie AH, Kerr JF and Currie AR: Cell death: the significance of apoptosis. Int Rev Cytol 68: 251-306, 1980.
70. Paulovich AG and Hartwell LH: A checkpoint regulates the rate of progression through S phase in S. cerevisiae in response to DNA damage. Cell 82: 841-847, 1995.
71. Burma S and Chen DJ: Role of DNA-PK in the cellular response to DNA double-strand breaks. DNA Repair (Amst) 3: 909-918, 2004.
72. Rothkamm K and Lobrich M: Misrepair of radiation-induced DNA double-strand breaks and its relevance for tumorigenesis and cancer treatment. (Review) Int J Oncol 21: 433-440, 2002.